Desalination and Water Treatment
www.deswater.com

doi:10.5004/dwt.2019.23290

139 (2019) 191–201
January

Synthesis of Mg/Al layered double hydroxides from a sub-bituminous coal ash and their application in hexavalent chromium removal from aqueous solution

Dong-Xue Guo[a], Yun-Peng Zhao[a,*], Hui-Duo Yang[a], Shi-Feng Li[b], Xing Fan[a], Xian-Yong Wei[a]

[a]*Key Laboratory of Coal Processing and Efficient Utilization (Ministry of Education), China University of Mining & Technology, Xuzhou 221116, China, Tel. +86 516 83885951, email: 704937207@qq.com (D. Guo), Tel. +86 516 83885951, Fax 86 516 83591093, email: zhaoyp@cumt.edu.cn (Y. Zhao), Tel. +86 516 83885951, email: 1063966026@qq.com (H. Yang), fanxing@cumt.edu.cn (X. Fan), wei_xianyong@163.com (X. Wei)*

[b]*College of Chemical Engineering, Shenyang University of Chemical Technology, Shenyang 110142, China, email: li.shi.feng@163.com (S. Li)*

Received 25 February 2018; Accepted 15 October 2018

ABSTRACT

An Mg/Al layered double hydroxide (LDH-A) for hexavalent chromium Cr(VI) removal was successfully synthesized from a sub-bituminous coal ash. For comparison, another Mg/Al-LDH (LDH-B) was also synthesized from an analytically pure chemical reagent using a similar method. Their characteristics were analyzed by Fourier transformed infrared (FT-IR) spectroscopy, X-ray diffraction (XRD), scanning electron microscopy, and N_2 Brunauer-Emmett-Teller surface area measurement. A batch of experiments were conducted to investigate the effects of the initial pH value, adsorption time, adsorbent dosage and initial Cr(VI) concentration on the adsorption capacities of Cr(VI) onto the LDHs in an aqueous solution. The adsorption capacity of Cr(VI) onto LDH-A was similar to that onto LDH-B, and the maximum adsorption capacity of Cr(VI) onto LDH-A was more than 66 mg/g at a pH of 3. The kinetics and isotherms of Cr(VI) adsorption onto the LDHs can be described with a pseudo-second-order kinetic model and a Freundlich isotherm, respectively.

Keywords: Layered double hydroxides; Chromium removal; Adsorption; Equilibrium; Kinetic

1. **Introduction**

The increasing discharge of heavy metals has attracted much attention across the world due to their high toxicity to humans and the environment [1]. One major heavy metal contaminant, hexavalent chromium Cr(VI), originates mainly in several industrial processes including electroplating, leather tanning, textile production, metal finishing and alloying [2]. It has been reported that Cr(VI) can penetrate the cell wall and affect DNA transcription, resulting in cancer and other serious illnesses [3,4]. Thus, the allowable concentration of chromium in industrial wastewater has been limited to below 0.1 mg/L by USEPA [5]. Current approaches to remove Cr(VI) from wastewater include adsorption, membrane filtration, chemical reduction and precipitation, and biological degradation. Among these approaches, adsorption is regarded as the most promising and widely used technique due to its low cost, high efficiency, and environmental friendliness [6].

Sub-bituminous coal is the major type of coal used in China, and the improper disposal of the ash from sub-bituminous coal combustion has caused several problems such as the appropriation of land and the contamination of soil, water and air because of the high alkalinity of its leachate and very small size [7,8]. Usually, coal ash is used for cement and concrete production, embankments, sludge stabilization, and soil treatment for agriculture [9]. Synthesizing adsorbents is an alternative approach to recycle and reuse coal ash, which not only turns the ash into an environmentally beneficial material but also solves its disposal problem. Researchers have synthesized various types of zeolite from coal ash and used them to remove methylene blue, phosphate, cadmium and nickel from wastewater [7,10].

*Corresponding author.

Recently, using waste materials as the feedstock for adsorbent has attracted much attention due to its cost savings [11]. Zhang et al. [12] successfully synthesized an Mg-Al based hydrotalcite from oil shale ash and used it in uranium removal. Coal ash is composed mainly of SiO_2, Al_2O_3, CaO, Fe_2O_3, MgO, and a few other metallic oxides similar to oil shale ash, and thus it is suitable as raw material for producing hydrotalcite. Moreover, the amount of coal ash produced is far more than that of oil shale ash worldwide. Layered double hydroxides (LDHs), also referred to as hydrotalcite-like compounds, have attracted widespread attention as effective adsorbents. The general formula of LDHs is $[M_{1-x}^{2+}M_x^{3+}(OH)_2]^{x+}(A^{n-})_{x/n}\cdot mH_2O$, which includes octahedral brucite-like host layers (M^{2+}/M^{3+}: divalent and trivalent metal cations; x = 0.2–0.33), charge-balancing anions (A^{n-}), and interlayer water molecules [13–15]. Due to their lamellar structure, hierarchical pore structure, high surface area, and interlayer ion exchange capacity, LDHs are promising adsorbent materials for the removal of heavy metals ions in effluents [16–20]. To our best knowledge, there is still little information about the LDHs synthesized from coal ash and their use in chromium removal.

In this work, an Mg/Al-LDH (abbreviated LDH-A below) was successfully synthesized from a coal ash combining leaching and co-precipitation treatment. For comparison, another Mg/Al-LDH (abbreviated LDH-B below) was also prepared using $Al(NO_3)_3$ and $Mg(NO_3)_2$ as aluminum and magnesium sources, respectively. Then, the removal behaviors of Cr(VI) by these LDHs were evaluated.

2. Experimental methods

2.1. Treatment of sub-bituminous coal ash

Huozhou sub-bituminous coal, a typical coal used for power generation in China, was collected from Huoxi coal basin in Shanxi Province, China. This coal was pulverized to pass through a 200-mesh sieve (<74 μm) and burned in muffle furnace by slow-ashing (at 500°C for 0.5 h and then at 815°C for 1 h) according to the Chinese Standard (GB/T212-2001) to remove all the organic matrix. For convenience, the remaining coal ash is referred to as HZSBA. Table 1 shows the chemical composition of the HZSBA. The HZSBA (25 g) was acid-leached with a 30 wt.% nitric acid solution (100 mL) at 80°C for 6 h with constant stirring. After the reaction was completed, the leaching liquor was separated from the residue by vacuum filtration. The composition of the leaching liquor was determined using inductively coupled plasma mass spectrometry (Agilent 7900). The amounts of Ti, Mg, Fe, Ca and Al in the leaching liquor were 1.55, 2.3, 28.2, 45.5 and 104.5 μg/mL, respectively, while Si and other components were successfully separated by leaching.

Table 1
Composition of HZSBA, wt.% (dry base)

Component	% HZSBA	Component	% HZSBA
TiO_2	1.06	Fe_2O_3	6.79
MgO	1.27	CaO	12.65
Na_2O	0.16	Al_2O_3	35.22
K_2O	0.49	SiO_2	42.36

2.2. Preparation of Mg/Al LDHs

The magnesium nitrate solution (100 mL, 4 M) was added to the leaching liquor from the HZSBA to form solution A. NaOH (1 M, 150 mL) and Na_2CO_3 (0.5 M, 150 mL) were mixed together to form solution B. Solutions A and B were added to a 1000 mL flask with 100 mL of deionized water drop by drop at room temperature (25°C) with mechanical stirring (300 rpm). The pH of the reaction mixture was set to 9 by adjusting the dropping speed of solution B, and then the reaction mixture was aged for 24 h at 80°C, yielding a precipitate. Afterwards, the precipitate was filtrated, washed with deionized water and dried at 80°C for 48 h to yield Mg/Al-LDH (LDH-A). For comparison, Mg/Al-LDH (LDH-B) was also prepared using analytically pure $Al(NO_3)_3$ and $Mg(NO_3)_2$ as aluminum and magnesium sources via the same method.

2.3. Characterization

The chemical compositions of the HZSBA and LDHs were determined using an X-ray fluorescence spectrometer (Burker S8 TIGER). The crystallinity of the LDHs were characterized with an X-ray diffractometer (Bruker D8 Advanced). The procedures were conducted using Cu Kα radiation and a fixed power source (40 kV and 40 mA, λ = 0.15406 Å). Fourier transform infrared (FTIR) spectra were recorded on a Bruker EQUI-NOX55 spectrometer at a resolution of 2 cm^{-1} in the range of 4000–400 cm^{-1} using the KBr pellet technique. The surface morphology of the LDHs was analyzed using a scanning electron microscope (FEI Quanta 250). The BET measurement was performed on an adsorption instrument (BELSORP-max, Microtrac BET Company, Japan). To investigate the thermal stability of the LDHs, thermogravimetry analysis (TGA) was performed on a Mettler Toledo TGA/SDTA851e analyzer from 50 to 900°C with a heating rate of 10°C/min under an N_2 atmosphere at a constant flow rate of 60 mL/min.

2.4. Experimental procedure

The Cr(VI) stock solution was prepared by dissolving $K_2Cr_2O_7$ in pure water, and the working solutions for all adsorption experiments were freshly prepared from the stock solution. Standard acid (0.1 M HNO_3) and base solutions (0.1 M NaOH) were used for pH adjustment. The pH values of the working solutions were measured with a pH meter (SPSIC PHS-25, China) using a combined glass electrode. All adsorption experiments were conducted in a series of conical flasks (250 mL) held in a constant-temperature bath with constant magnetic stirring (200 rpm). Doses of adsorbents were added to 100 mL of the Cr(VI) solution with given concentrations and pH values. The Cr(VI) concentration in the supernatant was analyzed using an INESA 4510F atomic absorption spectrophotometer according to the standard method (American Public Health Association, 2012). All assays were performed in triplicate to ensure that variance in the data was within 5%, and only mean values

are presented. The adsorption capacity (q_t, mg/g) at adsorption time t and the equilibrium adsorption capacity (q_e, mg/g) were calculated as follows:

$$q_t = \frac{(c_0 - c_t)}{m} V \quad (1)$$

$$q_e = \frac{(c_0 - c_e)}{m} V \quad (2)$$

where C_0, C_t and C_e (mg/L) are the concentrations of Cr(VI) in solution at the initial time, adsorption time t and adsorption equilibrium time, respectively; m (mg) is the dosage of the LDHs, and V (L) is the volume of working solution.

To improve the process economics, the Cr(VI)-loaded LDHs were regenerated. In the first cycle, the adsorbent was dispersed in 100 mg/L of Cr (VI) solution for 4 h at 80°C, and then the Cr (VI)-loaded adsorbent was separated by filtration and rinsing with deionized water and dried at 80ºC overnight. Subsequently, the Cr(VI) saturated adsorbent was mixed with the mixture solution of NaOH (0.1 mol/L) and Na_2CO_3 (0.1 mol/L) and placed on a shaker at 200 rpm for 4 h at 25°C to evaluate the Cr(VI) desorption. Finally, the adsorbent was filtered, washed with deionized water and dried at 80°C overnight. The regenerated adsorbent continued to adsorb Cr(VI) under the same conditions.

3. Results and discussion

3.1. Characterization of the LDHs

As shown in Table S1, the elemental composition of LDH-A is similar to that of LDH-B, and the ratios of Al^{3+} to Mg^{2+} in LDH-A and LDH-B are 0.2678 and 0.2554, respectively. As shown in Fig. 1, the diffraction pattern of LDH-A shows a series of peaks indexed (003), (006), (009), (015), (018), (110) and (113) located at 10.2°, 20.0°, 34.7°, 38.4°, 46.3°, 61.0° and 61.9°, which are similar to those of LDH-B and basically consistent with PDF card (JCPDS No. 22-0700). The (003) and (006) crystal planes indicate that LDH-A is a well-crystallized hydrotalcite-like compound [21], while the lower sharpness and intensity of the reflections indicate the purity and crystallinity of LDH-A are lower than those of LDH-B.

Fig. 2 shows that the absorption bands in the FT-IR spectra of LDH-A are similar to those of LDH-B. The intense broad band between 3600 and 3200 cm^{-1} was associated with the stretching vibration of interlayer hydroxyl groups and surface water molecules [22]. The peak observed near 1620 cm^{-1} originated from bending deformation of interlayer water molecules [12]. The narrow band at 1382 cm^{-1} is due to asymmetric stretching vibration of interlayer NO_3^-. The bands in the low-frequency region are ascribed to stretching vibrations of Al-OH at 795 cm^{-1} and Mg-OH at 627 cm^{-1} and to deformation vibration of HO-Mg-Al-OH at 447 cm^{-1} [23,24]. As shown in Fig. 3, both the LDHs show the characteristics of plate-like morphology, although the lamellar structure of LDH-A is more disordered than that of LDH-B due to its lesser purity and crystallinity.

Thermalgravimetric/differential thermogravimetric (TG/DTG) curves are shown in Fig. S1. The weight loss before 230°C corresponded to the removal of water from the surface and the interlayer, and the weight loss that occurred from 230 to 500°C corresponded to the decomposition of carbonate anions and desorption of water produced by dihydroxylation [22]. The peak temperature of LDH-A is slightly higher than that of LDH-B, reflecting its greater thermal stability, and the total weight loss of LDH-A is higher than that of LDH-B, indicating its higher content of interlayer water, hydroxyl groups or carbonate anions.

As shown in Figs. 4a and b, the adsorption branches of the isotherms are below the desorption branches, and a hysteresis hoop for each isotherm is clearly visible since the pore constrictions slowed down nitrogen desorption [25]. Based on the IUPAC classification of adsorption isotherms, the N_2 adsorption-desorption isotherms of the LDHs are of type IV, implying the simultaneous presence of micro- and mesoporous. The hysteresis loop of LDH-B is of type H1 at relatively high pressures between 0.7 and 1.0, which

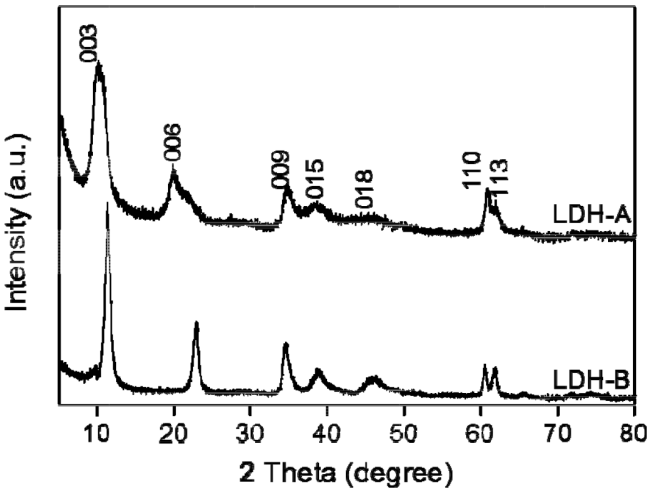

Fig. 1. XRD patterns of LDH-A and LDH-B.

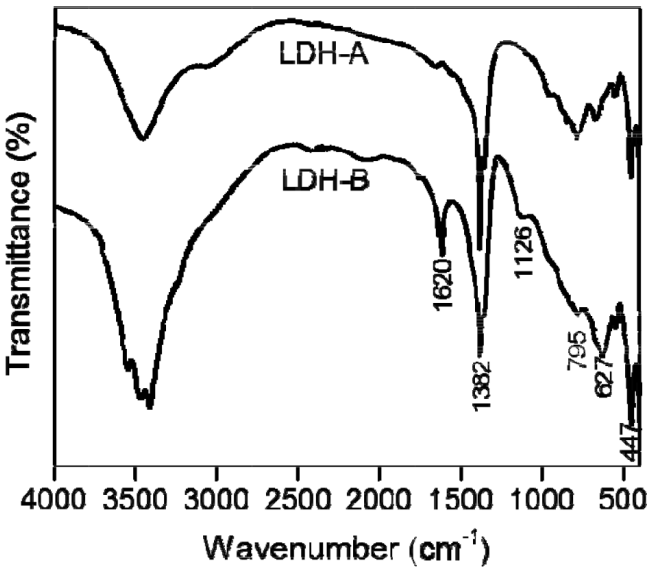

Fig. 2. FT-IR spectra of LDH-A and LDH-B.

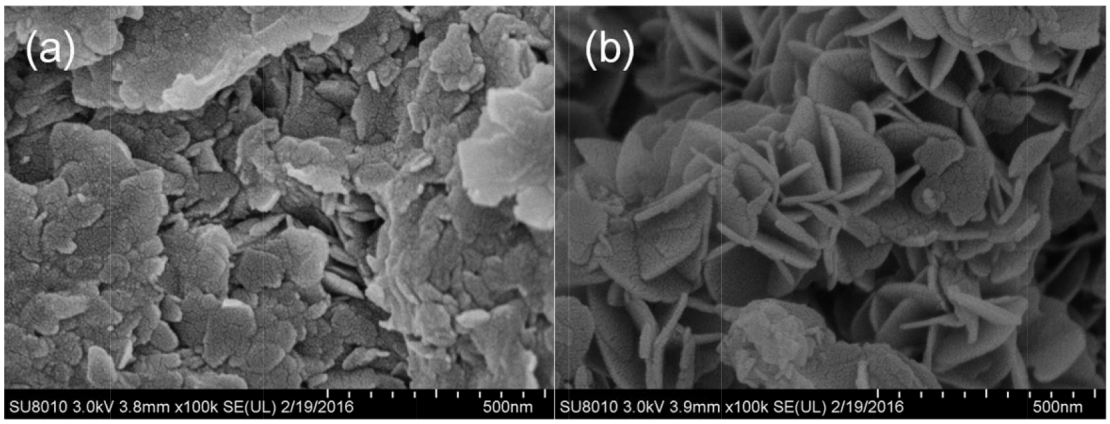

Fig. 3. SEM images of LDH-A (a) and LDH-B (b).

indicates that LDH-B possesses a narrow pore diameter distribution. Nevertheless, the hysteresis loop of LDH-A is of type H2 across a broad pressure range between 0.4 and 1.0, suggesting that LDH-A has a broad pore diameter distribution. There exist only two narrow peaks between 10 and 70 nm in the pore diameter distribution curve of LDH-B, whereas the pore diameter distribution of LDH-A is more dispersed. As listed in Table 2, the BET surface area of LDH-A is as high as 204 m^2/g, implying that it can provide sufficient active adsorption sites.

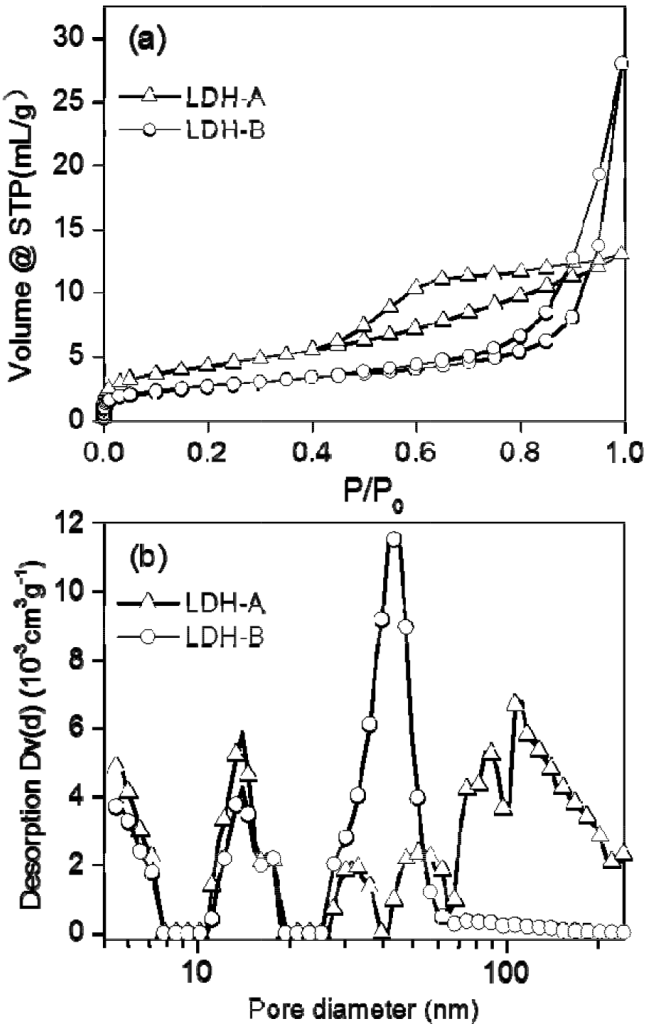

Fig. 4. Nitrogen adsorption–desorption isotherms (a) and pore diameter distribution curves (b).

3.2. *Effect of adsorption conditions*

The pH of an aqueous solution is an important factor in the adsorption of heavy metals [14]. As shown in Fig. 5a, the adsorption capacity of Cr(VI) first increases with an increase in pH from 1 to 3 and thereafter decreases with further increases in pH. The maximum adsorption capacities of Cr(VI) onto LDH-A and LDH-B at pH = 3 are 48.55 and 49.25 mg/g, respectively. Therefore, pH = 3 was taken as the optimal value for further adsorption experiments. It was earlier observed that the forms of dissolved ions and the surface chemistry of an adsorbent are significantly controlled by the pH [26,27]. Yavuz et al. [28] found that different complexes of Cr(VI) can form in aqueous solutions with different pH values. $Cr_2O_7^{2-}$ is the predominant form of Cr(VI) below a pH of 6.0, while the concentration of CrO_4^{2-} increases with increasing pH. An adsorbent surface can be protonated with numerous H^+ ions at a low pH, which favors the diffusion of $HCrO_4^-$ and their electrostatic attraction. The suppression of Cr(VI) uptake onto the LDHs at pH < 3 might be attributed to the less-negative charge on the surface of the LDHs, which was unfavorable for adsorbing positively charged ions [29]. Additionally, the acid-dissolution of the LDHs at pH < 3 is one reason for the low adsorption capacity, especially at pH = 1. The $HCrO_4^-$ gradually converts to CrO_4^{2-} with increasing pH. Moreover, the competition adsorption of excess OH^- ions with $HCrO_4^-$ occurs at high pH values.

Fig. 5b shows that the adsorption capacity of Cr(VI) increases with increases in the LDHs dosage from 0.2 to 0.6 mg/mL because of the increase in adsorbent surface area and adsorption sites. Nevertheless, the adsorption capacity of Cr(VI) significantly decreases with the increases in the LDH dosage. The results are consistent with findings published by Namasivayam et al. [30]. They found that the adsorption capacity of chromium significantly decreased with increases in adsorbent dosage, probably due to an overlap of adsorption sites resulting from overcrowding

Table 2
Pore parameters of the LDHs

Sample	S_{BET} [a] (m^2/g)	V_{total} [b] (cm^3/g)	V_{mic} [c] (cm^3/g)	V_{mec} [d] (cm^3/g)	D_{BJH} [e](nm)
LDH-A	204.0	0.26	0.08	0.24	35.87
LDH-B	273.2	1.19	0.11	0.79	17.38

[a]BET surface area; [b]Total pore volume; [c]Micropore volume; [d]Macropore volume; [e]BJH desorption average pore diameter.

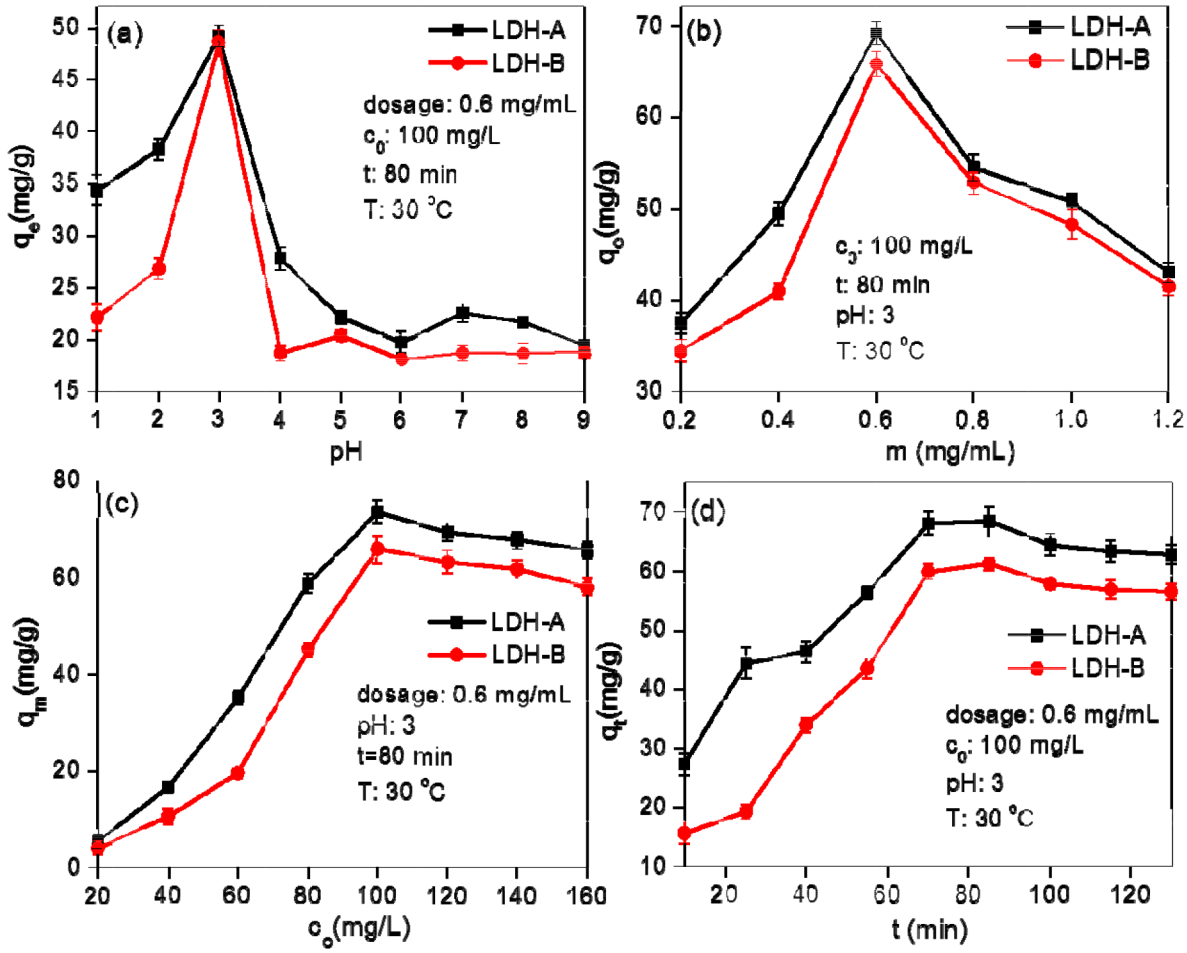

Fig. 5. Effects of the adsorption conditions on Cr(VI) adsorption by the LDHs: (a) pH; (b) adsorbent dosage; (c) initial chromium concentration; (d) adsorption time.

of adsorbent particles. As shown in Fig. 5c, the adsorption capacity of Cr(VI) onto the LDHs increases with increases in Cr(VI) concentration from 0.2 to 1.0 mg/mL. Gode and Jacques et al. [31,32] found that the adsorption capacity rapidly increased to a certain level and remained stable with further increases in Cr(VI) concentration. However, the adsorption capacity onto the LDHs decreases slightly with further increases in Cr(VI) concentration, indicating that there exist high-energy adsorption sites to promote the adsorption of Cr(VI) onto the LDHs at low equilibrium concentrations. The effect of adsorption time was investigated for determining the equilibration time of the Cr(VI) adsorption onto the LDHs and discussing the adsorption kinetics. Fig. 5d shows that the adsorption capacity of Cr(VI) initially increases with time and then reaches a plateau at ca. 80 min, implying that an adsorption equilibrium of Cr(VI) onto the LDHs could be obtained after a relatively short time period.

The adsorption performance of Cr(VI) onto LDH-A and other adsorbents reported in the literature are listed in Table 3. The q_m of LDH-A is clearly higher than that of the other adsorbents, suggesting that it possesses good potential for removal of Cr(IV) from wastewater.

3.3. Adsorption kinetics

To further investigate the interaction mechanism, a pseudo-first-order model and a pseudo-second-order model were applied to simulate the adsorption kinetics of Cr(VI) onto the LDHs using the data from Fig. 6d. The two kinetic models are as follows [38]:

Table 3
Maximum adsorption capacity of various adsorbents for Cr(VI) removal from aqueous solutions

Adsorbent	Adsorption capacity	pH	Reference
LDH-A	66.12	3	This work
Gourd ash	18.7	1	[33]
Modified corn stalk	112	4.91	[34]
Chitosan flakes	22.09	3	[35]
Sawdust	48.19	2	[36]
Carboxymethyl cellulose	5.1	2	[37]

$$\ln\left(q_e - q_t\right) = \ln q_e - k_1 t \tag{3}$$

$$\frac{t}{q_t} = \frac{1}{k_2 q_e^{\,2}} + \frac{t}{q_e} \tag{4}$$

where k_1 and k_2 are the kinetic adsorption rate constants of the pseudo-first-order and pseudo-second-order models, respectively.

Based on the forms of the equations, $ln(q_e - q_t)$ as the ordinate and t as the abscissa were used in linear fitting to produce the pseudo-first-order parameters, and t/q_t as the ordinate and t as the abscissa were used in linear fitting to produce the pseudo-second-order parameters [38]. The rate constants and regression coefficients from the fitting curves (Fig. 6) are listed in Table 4. It is clear that the adsorption kinetics follow the pseudo-second-order kinetic model ($R^2 > 0.98$) better than the pseudo-first-order model ($R^2 < 0.80$).

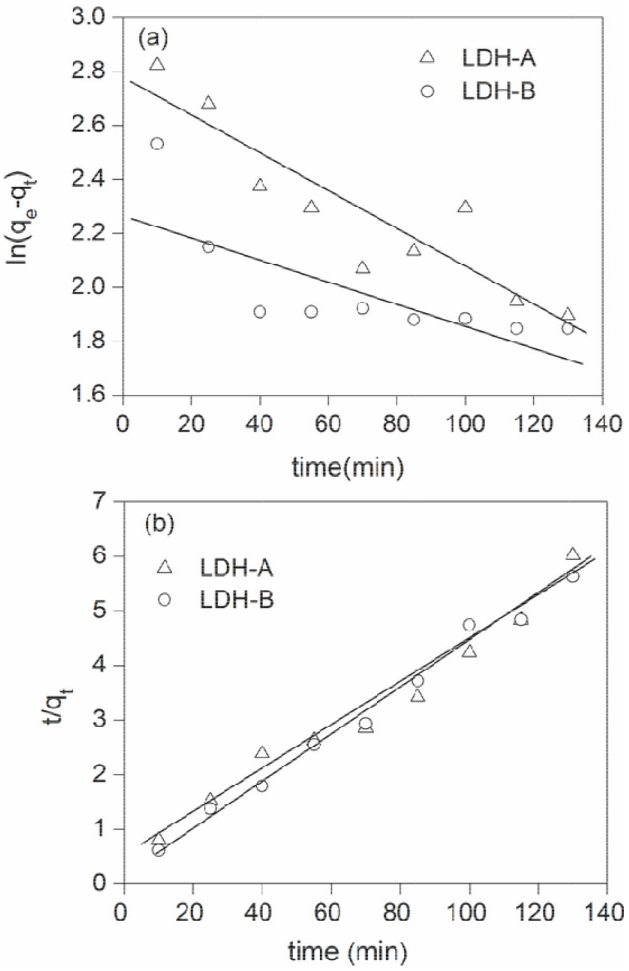

Fig. 6. Pseudo-first-order (a) and pseudo-second-order (b) adsorption kinetics of chromium adsorption onto the LDHs.

3.4. Adsorption isotherms and thermodynamic parameters

The influence of temperature on Cr(VI) ion adsorption onto the LDHs was investigated at temperatures ranging from 293 to 313 K. As shown in Fig. 7, the maximum Cr(VI) adsorption on the LDHs occurs at 303 K (30°C). The increase in temperature decreases the solution viscosity and accelerates the diffusion rate of the adsorbate molecules across the external boundary layer and internal pores of the LDHs, but the kinetic energy of adsorbate molecules increases with increasing temperature, which weaken the adsorbate-adsorbent interaction [15].

Both Langmuir and Freundlich isotherms models were used to simulate the adsorption isotherms at 303 K. The two models can be described as Eqs. (5) and (6), respectively [39,40]:

$$\frac{c_e}{q_e} = \frac{1}{q_m} c_e + \frac{1}{b q_m} \tag{5}$$

$$\log q_e = \frac{1}{n} \log c_e + \log k_f \tag{6}$$

where b (L/mg) is the Langmuir constant, q_m (mg/g) is the maximum adsorption capacity, n is a constant related to the adsorption intensity, and k_f is a constant related to the adsorption capacity of the adsorbent. As shown in Fig. 8 and Table 5, the plots of ln q_e vs ln c_e are linear and have good correlation coefficients, indicating the applicability of the Freundlich isotherm model to the adsorption [22]. The n values obtained from the Freundlich model for the Cr(VI)

Table 4
Kinetic parameters of the adsorption of chromium onto the LDHs

Adsorbent	Pseudo-first-order			Pseudo-second-order		
	k_1 (L·min^{-1})	q_e (mg·g^{-1})	R^2	k_2 (g·mg^{-1}·min^{-1})	q_e (mg·g^{-1})	R^2
LDH-A	0.083	78.65	0.794	0.052	37.17	0.982
LDH-B	0.074	65.80	0.517	0.054	46.73	0.986

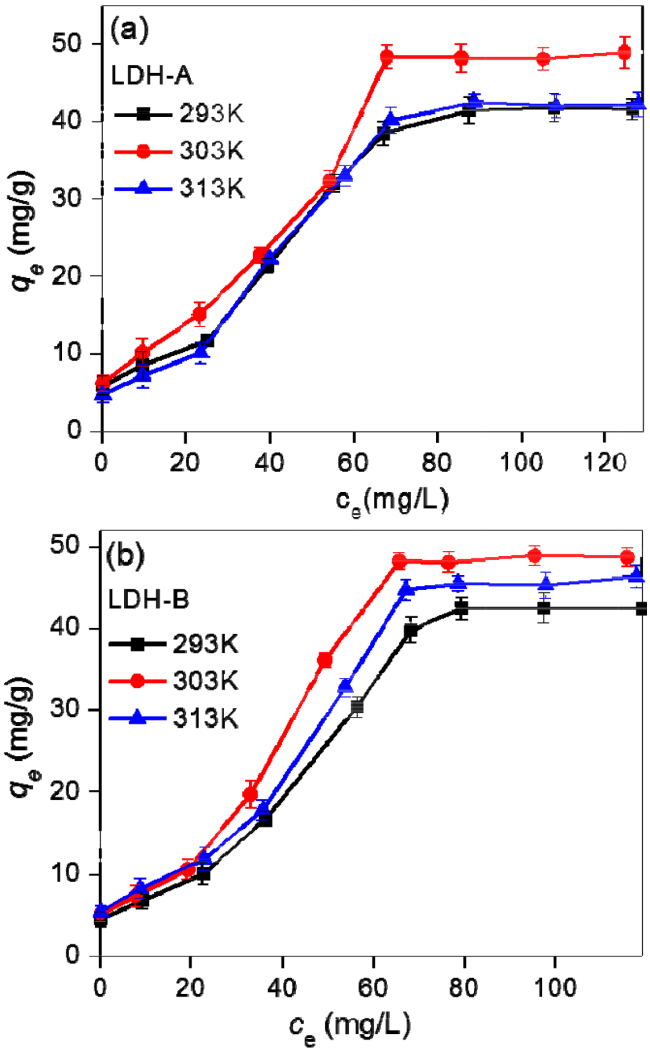

Fig. 7. Adsorption isotherms of Cr(VI) adsorption onto the LDHs at various temperatures, (a) LDH-A; (b) LDH-B.

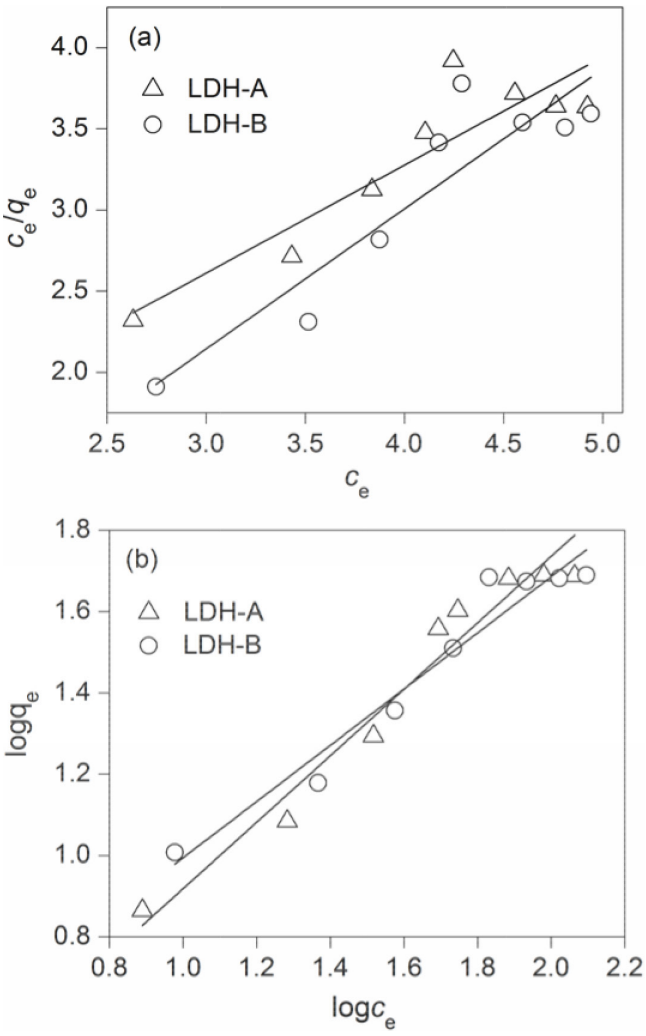

Fig. 8. Linear plots of Langmuir (a) and Freundlich (b) isotherms of Cr(VI) adsorption onto the LDHs.

Table 5
Isotherm parameters of the adsorption of Cr(VI) onto the LDHs

Adsorbent	Langmuir model			Freundlich model		
	b (L·mg^{-1})	q_m (mg·g^{-1})	R_L^2	n	k_f	R_F^2
LDH-A	0.007	125.00	0.388	1.22	1.11	0.908
LDH-B	0.010	99.01	0.765	1.45	1.35	0.940

adsorption were above 1, which implies that beneficial adsorption occurred on the heterogeneous surfaces of the LDHs [26].

The energy and entropy were considered to determine the process that would occur spontaneously [38]. The adsorption thermodynamic parameters including the standard entropy ($\Delta H°$), free energy ($\Delta G°$), and standard entropy ($\Delta S°$) were calculated using the following equations [41]:

$$\Delta G^o = -RT\ln K \tag{7}$$

$$\Delta S^o = \frac{\left(\Delta H^o - \Delta G^o\right)}{T} \tag{8}$$

where T, R and K are the absolute temperature (K), gas constant (8.314 J·mol^{-1}·K^{-1}) and Freundlich adsorption constant, respectively. $\Delta H°$ and $\Delta S°$ can be obtained directly from the slope and intercept of the linear plot of ln$K$ vs. $1/T$. As listed in Table 6, the positive values of $\Delta H°$ indicate that the adsorption is endothermic, while the $\Delta H°$ value is lower than 4 kJ/mol, implying that the adsorption involves only physical adsorption and/or complexation.

Table 6
Thermodynamic parameters of the adsorption of Cr(VI) onto the LDHs

Temperature (K)	LDH-A			LDH-B		
	ΔG^o (kJ/mol)	ΔH^o (kJ/mol)	ΔS^o (J/mol)	ΔG^o (kJ/mol)	ΔH^o (kJ/mol)	ΔS^o (J/mol)
293	–2.97			–3.53		
303	–3.07	3.43	21.84	–3.65	–3.50	23.99
313	–3.17			–3.77		

The negative values of $\Delta G°$ suggest that the adsorption of Cr(VI) onto the LDHs is thermodynamically feasible and spontaneous, while the positive value of $\Delta S°$ demonstrates that the degree of disorder increases with the species number increasing at the solid/liquid interface when the Cr(VI) from the aqueous solution transfer to the surface of the LDHs [22,41].

3.5. Desorption and regeneration of Cr(VI)-loaded LDHs

The desorption ratio (DR %) was determined using Eq. (10) [42,43]:

$$DR\% = \frac{\text{Amount of desorbed metal ion}}{\text{Amount of adsorbed metal ion}} \times 100 \quad (10)$$

The Cr(VI) adsorption capacity onto the LDHs through four regeneration cycles is illustrated in Fig. S4. The maximum adsorption capacities of Cr(VI) onto LDH-A and LDH-B decreased by 34.4 and 32.5 mg/g, respectively. The fact that the adsorption capacity remained above 30 mg/g indicates the strong interaction between Cr(VI) and the adsorbents. However, 68.72% and 63.55% of the adsorbed Cr(VI) was desorbed in the first adsorption–desorption cycles using LDH-A and LDH-B, and these amounts decreased to 42.13% and 40.64%, respectively, after the fourth desorption. The total reductions after four cycles were 26.59% and 22.91%, respectively, indicating that the LDHs have potential for use in water treatment.

3.6. Characterization of the cr-loaded LDHs

As shown in Fig. S2, all the adsorption bands in the FTIR spectra of LDHs after chromium ion adsorption shifted slightly. For example, the band at 795 cm^{-1} shifted to 887 cm^{-1} after adsorption, suggesting the adsorption of chromium ion on the active sites of Al-O bonds [7]. SEM images and energy-dispersive X-ray (EDS) patterns of the Cr(VI)-loaded LDHs are shown in Fig. S3. The morphology of the Cr(VI)-loaded LDHs is similar to that of the LDHs before the adsorption of Cr(VI) (Fig. 3), indicating the good structural stability of the LDHs. EDS patterns of the Cr(VI)-loaded LDHs show the clear signals of Cr, which provided direct evidence for Cr(VI) adsorption onto the surfaces of the LDHs.

4. Conclusions

In this work, an Mg/Al LDH (LDH-A) was successfully synthesized from a sub-bituminous coal ash. Analyses of the structural and morphological properties reveal that LDH-A is an Mg-Al based hydrotalcite compound featuring a lamellar morphology and large surface area (204 m^2/g). The maximum adsorption capacity of Cr(VI) onto LDH-A is 66.12 mg/g. The adsorption can be simulated with a pseudo-second-order reaction model and a Freundlich isotherm model. The thermodynamic parameters indicate that the adsorption of Cr(VI) onto LDH-A is an exothermic and spontaneous process and involves only physical adsorption or/and complexation.

Acknowledgments

This work was supported by the National Natural Science Foundation of China (Grant 21878325), the Fundamental Research Funds for the Central Universities (China University of Mining and Technology, 2017XKZD10) and a Project Funded by the Priority Academic Program Development of Jiangsu Higher Education Institutions.

References

[1] D.L. Huang, G.M. Chen, G.M. Zeng, P. Xu, M. Yan, C. Lai, C. Zhang, N.J. Li, M. Cheng, X.X. He, Y. He, Synthesis and application of modified zero-valent iron nanoparticles for removal of hexavalent chromium, Water Air Soil Poll., 226 (2015) 49–57.
[2] V.K. Gupta, S. Agarwal, T.A. Saleh, Chromium removal by combining the magnetic properties of iron oxide with adsorption properties of carbon nanotubes, Water Res., 45 (2011) 2207–2212.
[3] P.N. Singh, D. Tiwary, I. Sinha, Chromium removal from aqueous media by super paramagnetic starch functionalized maghemite nanoparticles, J. Chem. Sci., 127 (2015) 1967–1976.
[4] S. Rengarai, K.H. Yeon, S.H. Moon, Removal of chromium from water and wastewater by ion exchange resins, J. Hazard. Mater., 87 (2001) 273–287.
[5] L. Dupont, E. Guillon, Removal of hexavalent chromium with a lignocellulosic substrate extracted from wheat bran, Environ. Sci. Technol., 37 (2003) 4235–4241.
[6] A.G. Yavuz, E.D. Atalay, A. Uygun, F. Gode, E. Aslan, A comparison study of adsorption of Cr(VI) from aqueous solutions onto alkyl-substituted polyaniline/chitosan composites, Desalination, 279 (2011) 325–331.
[7] H.X. Wang, X.R. Wang, Z.H. Xu, M.L. Zhang, Synthetic zeolite from coal bottom ash and its application in cadmium and nickel removal from acidic wastewater, Desal. Water Treat., 57 (2016) 26089–26100.
[8] N. Koukouzas, C. Ketikidis, G. Itskos, Heavy metal characterization of CFB-derived coal fly ash, Fuel Process. Technol., 92 (2011) 441–446.
[9] L.C. Ram, R.E. Masto, An appraisal of the potential use of fly ash for reclaiming coal mine spoil, J. Environ. Manage., 91 (2010) 603–617.

[10] J. Xie, L. Lai, L.D. Lin, D.Y. Wu, Z.J. Zhang, H.N. Kong, Phosphate removal from water by a novel zeolite/lanthanum hydroxide hybrid material prepared from coal fly ash, J. Environ. Sci. Health, Part A: Environ. Sci. Eng., 50 (2015) 1298–1305.
[11] P.X. Wu, Z.W. Liao, H.F. Zhang, J.G. Guo, Adsorption of phenol on inorganic-organic pillared montmorillonite in polluted water, Environ. Int., 26 (2001) 401–407.
[12] H.S. Zhang, J. Wang, B. Zhang, Q. Liu, S.N. Li, H.J. Yan, L.H. Liu, Synthesis of a hydrotalcite-like compound from oil shale ash and its application in uranium removal, Colloids Surf., A 44 (2014) 129–137.
[13] R.Z. Ma, Z.P. Liu, K. Takada, N. Iyi, Y. Bando, T. Sasaki, Synthesis and exfoliation of Co^{2+}-Fe^{3+} layered double hydroxides: An innovative topochemical approach, J. Am. Chem. Soc., 129 (2007) 5257–5263.
[14] X.L. Song, Y.H. Wu, Simultaneous adsorption of chromium (VI) and phosphate by calcined Mg-Al-CO3 layered double hydroxides, Bull. Korean Chem. Soc., 35 (2014) 1817–1824.
[15] H.D. Yang, Y.P. Zhao, S.F. Li, X. Fan, X.Y. Wei, Z.M. Zong, Removal of hexavalent chromium from aqueous solution by calcined Zn/Al-LDHs, Water Sci. Technol., 74 (2016) 229–235.
[16] C.S. Lei, X.F. Zhu, B.C. Zhu, C.J. Jiang, Y. Le, J.G. Yu, Superb adsorption capacity of hierarchical calcined Ni/Mg/Al layered double hydroxides for Congo red and Cr(VI) ions, J. Hazard. Mater., 321 (2017) 801–811.
[17] F.R. Peligro, I. Pavlovic, R. Rojas, C. Barriga, Removal of heavy metals from simulated wastewater by in situ formation of layered double hydroxides, Chem. Eng. J., 306 (2016) 1035–1040.
[18] H. Chen, G. Qian, X.X. Ruan, R.L. Frost, Removal process of nickel (II) by using dodecyl sulfate intercalated calcium aluminum layered double hydroxide, Appl. Clay. Sci., 132 (2016) 419–424.
[19] T. Türk, I. Alp, Arsenic removal from aqueous solutions with Fe-hydrotalcite supported magnetite nanoparticle, J. Ind. Eng. Chem., 20 (2014) 732–738.
[20] F.L. Ling, L. Fang, Y. Lu, J.M. Gao, F. Wu, M. Zhou, B.S. Hu, A novel CoFe Layered double hydroxides adsorbent: High adsorption amount for methyl orange dye and fast removal of Cr(VI), Micropor. Mesopor. Mat., 234 (2016) 230–238.
[22] Q.T. Zhang, Q.R. Li, H.Y. Xiao, H.X. Lu, Y.M. Zhou, Synthesis of Li-Al layered double hydroxides (LDHs) for efficient fluoride removal, Ind. Eng. Chem. Res., 51 (2012) 11490–11498.
[23] L.F. Bo, Q.R. Li, Y.H. Wang, L.L. Gao, X.H. Hu, J.H. Yang, Adsorptive removal of fluoride using hierarchical flower-like calcined Mg-Al layered double hydroxides, Environ. Prog. Sustain., 35 (2016) 1420–1429.
[24] J.T. Kloprogge, R.L. Frost, Fourier transform infrared and raman spectroscopic study of the local structure of Mg-, Ni-, and Co-hydrotalcites, J. Solid State Chem., 146 (1999) 506–515.
[25] J.T. Kloprogge, L. Hickey, R.L. Frost, Heating stage Raman and infrared emissions spectroscopic study of the dehydroxylation of synthetic Mg-hydrotalcite. Appl. Clay Sci., 18 (2001) 37–49.
[26] W.Q. Cai, J.G. Yu, B. Cheng, B.L. Su, M. Jaroniec, Synthesis of boehmite hollow core/shell and hollow micro spheres via sodium tartrate-mediated phase transformation and their enhanced adsorption performance in water treatment, J. Phys. Chem. C., 113 (2009) 14726–14739.
[27] D.J. Kang, X.L. Yu, S.R. Tong, M.F. Ge, J.C. Zuo, C.Y. Cao, W.G. Song, Performance and mechanism of Mg/Fe layered double hydroxides for fluoride and arsenate removal from aqueous solution, Chem. Eng. J., 228 (2013) 731–740.
[28] J.G. Zhou, Y.F. Wang, J.T. Wang, W.M. Qiao, D.H. Long, L.C. Ling. Effective removal of hexavalent chromium from aqueous solutions by adsorption on mesoporous carbon micro spheres, J. Colloid Interf. Sci., 462 (2016) 200–207.
[29] A.G. Yavuz, E.D. Atalay, F. Gode, E. Aslan, A comparison study of adsorption of Cr(VI) from aqueous solutions onto alkyl-substituted polyaniline/chitosan composites, Desalination, 279 (2011) 325–331.
[30] C.M. Liu, P.X. Wu, Y.J. Zhu, L. Tran, Simultaneous adsorption of Cd^{2+} and BPA on amphoteric surfactant activated montmorillonite, Chemosphere, 144 (2016) 1026–1032.
[31] C. Namasivayam, D. Prabha, M. Kumutha, Removal of direct red and acid brilliant blue by adsorption on to banana pith, Bioresour. Technol., 64 (1998) 77–79.
[32] F. Gode, E. Moral, Column study on the adsorption of Cr(III) and Cr(VI) using Pumice, Yarıkkaya brown coal, Chelex-100 and Lewatit MP 62, Bioresour. Technol., 99 (2008) 1981–1991.
[33] R.A. Jacques, R. Bernardi, M. Caovila, E.C. Lima, F.A. Pavan, J.C.P. Vaghetti, C. Airoldi, Removal of Cu(II), Fe(III), and Cr(III) from aqueous solution by aniline grafted silica gel, Sep. Sci. Technol., 42 (2007) 591–609.
[34] K.M. Sreenivas, M.B. Inarkar, S.V. Gokhale, S.S. Lele, Re-utilization of ash gourd (Benincasa hispida) peel waste for chromium (VI) biosorption: Equilibrium and column studies, J. Environ. Chem. Eng., 2 (2014) 455–462.
[35] S.H. Chen, Q.Y. Yue, B.Y. Gao, Q. Li, X. Xu, K.F. Fu, Adsorption of hexavalent chromium from aqueous solution by modified corn stalk: A fixed-bed column study, Bioresour. Technol., 113 (2012) 114–120.
[36] Y.A. Aydın, N.D. Aksoy, Adsorption of chromium on chitosan: Optimization, kinetics and thermodynamics, Chem. Eng. J., 151 (2009) 188–194.
[37] N.K. Hamadi, X.D. Chen, M.M. Farid, M.G.Q. Lu, Adsorption kinetics for the removal of chromium(VI) from aqueous solution by adsorbents derived from used tyres and sawdust, Chem. Eng. J., 84 (2001) 95–105.
[38] M.Y. Arıca, G. Bayramoglu, Cr(VI) biosorption from aqueous solutions using free and immobilized biomass of Lentinus sajor-caju: preparation and kinetic characterization, Colloid Surface A., 253 (2005) 203–211.
[39] P.X. Wu, W.M. Wu, S.Z. Li, N. Xing, N.W. Zhu, P. Li, J.H. Wu, C. Yang, Z. Dang, Removal of Cd^{2+} from aqueous solution by adsorption using Fe- montmorillonite, J. Hazard. Mater., 169 (2009) 824–830.
[40] S. Mandal, S. Tripathy, T. Padhi, M.K. Sahu, R.K. Patel, Removal efficiency of fluoride by novel Mg–Cr–Cl layered double hydroxide by batch process from water, J. Environ. Sci., 25 (2013) 993–1000.
[41] L. Xiao, W. Ma, M. Han, Z. Cheng, The influence of ferric iron in calcined nano-Mg/Al hydrotalcite on adsorption of Cr(VI) from aqueous solution, J. Hazard. Mater., 186 (2011) 690–698.
[42] D.L. Guerra, R.R. Viana, C. Airoldi, Adsorption of mercury cation on chemically modified clay, Mater. Res. Bull., 44 (2009) 485–491.
[43] S. Jorfi, M.J. Ahmadi, S. Pourfadakari, N. Jaafarzadeh, R.D.C. Soltani, H. Akbari, Adsorption of Cr(VI) by natural clinoptilolite zeolite from aqueous solutions: Isotherms and kinetics, Pol. J. Chem. Technol., 19 (2017) 106–114.
[44] X.Y. Yuan, Y.F. Wang, J. Wang, C. Zhou, Q. Tang, X.B. Rao, Calcined graphene/MgAl-layered double hydroxides for enhanced Cr(VI) removal, Chem. Eng. J., 221 (2013) 204–213.

Supplementary Data

Table S1
Average elemental compositions of LDH-A and LDH-B, wt% (dry matter).

Component	LDH-A	LDH-B
C, H, O, N total	62.5362	70.0135
Si	0.0919	0.0579
Al	8.4671	6.6700
Fe	0.0918	0.0164
S	0.0198	0.0140
Mg	28.7824	23.2180
Zn	0.01080	0.01020

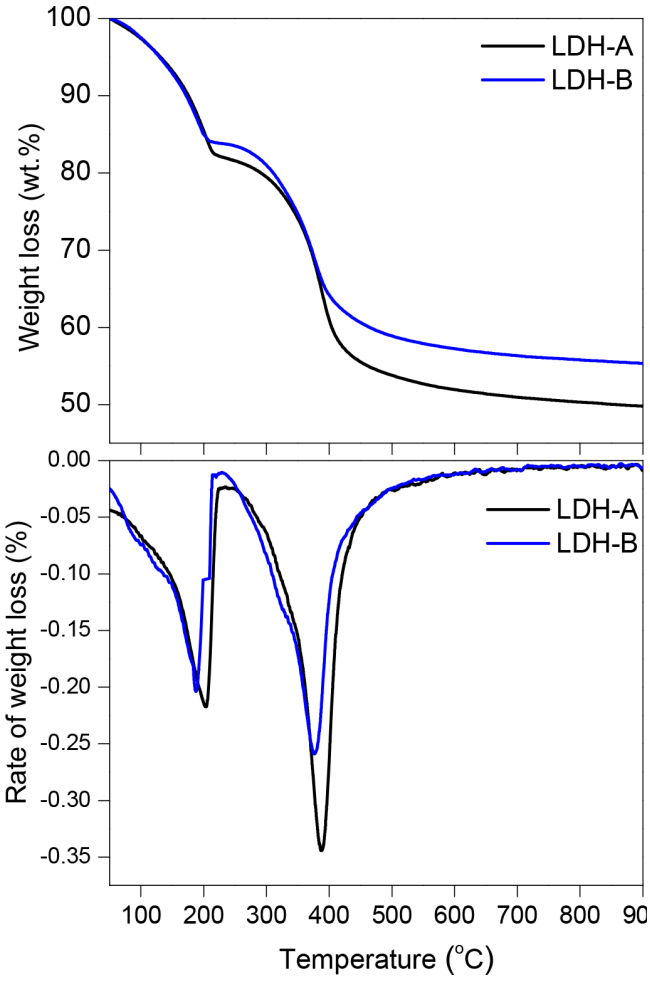

Fig. S1. TG/DTG curves of the LDHs.

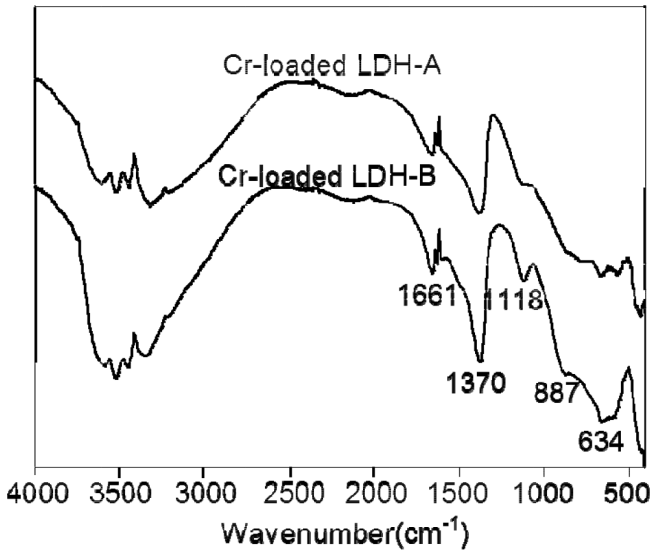

Fig. S2. FTIR spectra of Cr(VI)-loaded LDHs.

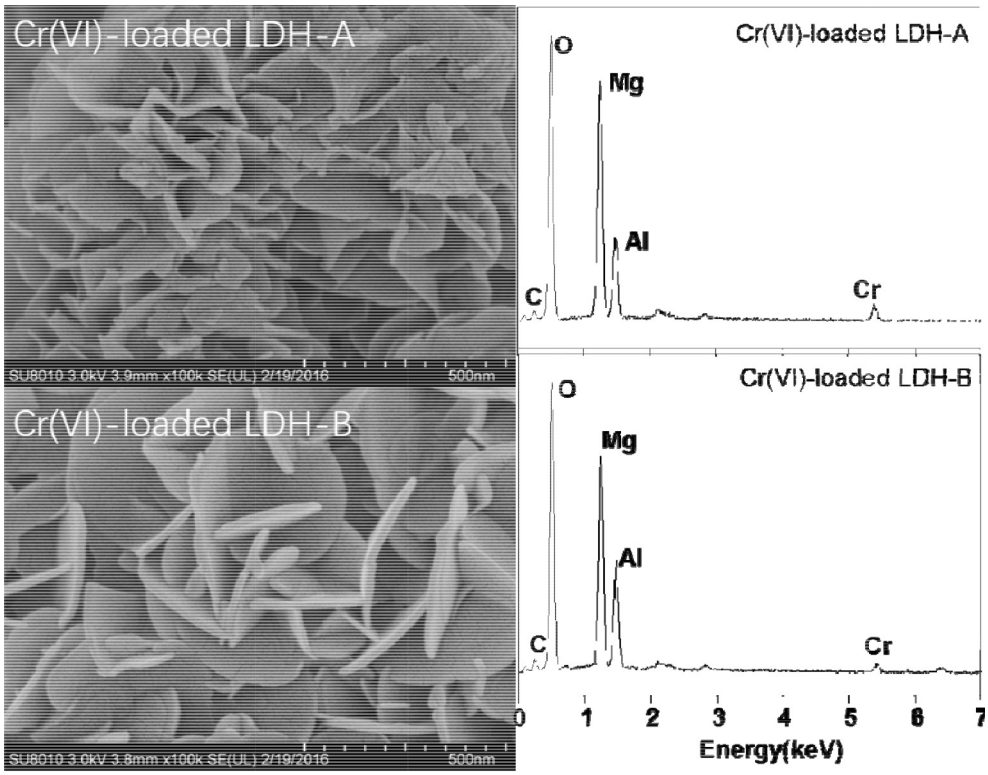

Fig. S3. SEM images and EDS analyses of Cr(VI)-loaded LDHs.

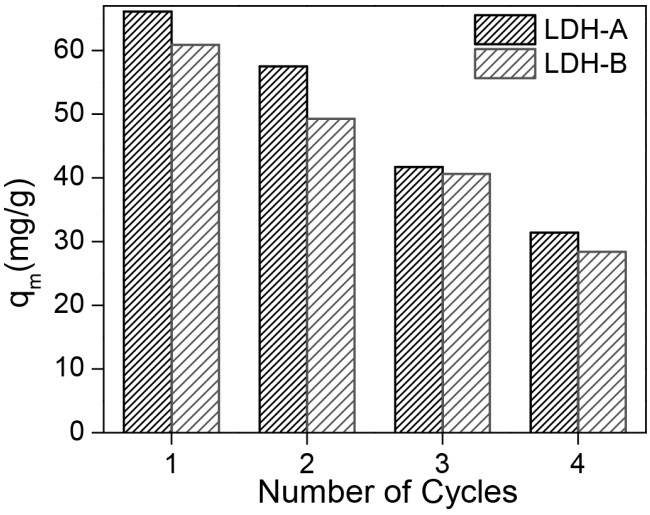

Fig. S4. Regeneration of LDHs